Applied Physics A (2019) 125:429
https://doi.org/10.1007/s00339-019-2705-7

Applied Physics A
Materials Science & Processing

Effect of bistrifluoromethane sulfonimide treatment on nickel/InAs contacts

Kazy F. Shariar[1] · Guangyang Lin[1] · Zijian Wang[2] · Peng Cui[1] · Jie Zhang[1] · Robert Opila[2] · Yuping Zeng[1]

Received: 25 February 2019 / Accepted: 8 May 2019 / Published online: 23 May 2019

Abstract
In this work, the effects of bis(trifluoromethane) sulfonimide (TFSI) (a superacid) surface treatment on electrical properties of nickel/InAs contacts and InAs material are investigated with transmission line measurements (TLMs). After TFSI treatments on bare InAs TLM patterns, the contact resistance between InAs and Ni contact increased. While for InAs TLM structure passivated with a ZrO_2 thin film, the total resistance of InAs decreased drastically after TFSI treatments. X-ray photoelectron spectroscopy measurements revealed that the TFSI reduced the indium oxide at the InAs/ZrO_2 interface. This novel passivation method can be adopted in III–V semiconductor device fabrication process to reduce contact resistance and, therefore, enhance device performances, providing a new guidance for III–V fabrication process technology.

1 Introduction

InAs-based devices have the potential to become the next generation of low-power and high-speed devices due to the unique features of InAs such as high electron mobility and narrow bandgap [1–3]. InAs has already been applied in RF devices such as planar high-electron-mobility transistors (HEMTs), although they suffer from high leakage current [4] due to its narrow bandgap. This shortcoming impedes the application of InAs in MOSFETs. With recent developments in the 3D architecture of FinFETs, more robust gate control is possible and the leakage current can be brought down to as little as 400 pA/μm [5], enabling InAs to be used for highly scaled logic devices.

Integration of InAs compound semiconductor devices on silicon to realize complementary metal–oxide–semiconductor field-effect transistor (CMOS)-compatible technology has been a very challenging topic. There are a couple of promising approaches to achieving III–V hetero-integration on Si. One approach is to use buffer layer on Si to directly grow III–V materials and another approach is a selective transfer of epitaxial InAs to the Si/SiO_2 surface. Although the transfer method prevents the lattice mismatch issue between III–V materials and Si, the quality of the material interfaces and the electrical properties of metal/III–V material contacts are still under investigation. Abundant surface or interface treatment methods using gases such as H_2/N_2 anneal, H_2S anneal, CF_4/O_2 plasma annealing, thermal oxidation and so on have been applied to improve the surface quality of semiconductors and their contacts with metals [6–15]. Additionally, various types of wet solutions have also been employed to treat the III–V semiconductor surfaces [16–19]. Bis(trifluoromethane) sulfonimide (TFSI) is one of the organic acids, which has extremely high Hammett number (~ 10^{10} times higher than nitric and sulfuric acids) and is a promising chemical candidate for surface treatment. Recently, TFSI was used to demonstrate near-unity photoluminescence quantum yield in MoS_2 by Amani et al. [20]. To the best of our knowledge, no study has been reported on TFSI as a surface treatment methodology for III–V materials. In this paper, for the first time, we investigate the effects of TFSI surface treatment on the InAs surface as well as Au/Ni/InAs contacts with transmission line measurements (TLMs).

2 Experimental details

InAs TLM patterns were fabricated on Si/SiO_2 substrate. Epitaxially grown single-crystal InAs films on GaSb substrate were used as donor substrate during the

✉ Yuping Zeng
yzeng@udel.edu

[1] Department of Electrical and Computer Engineering, University of Delaware, Delaware 19716, USA

[2] Department of Materials Science and Engineering, University of Delaware, Delaware 19716, USA

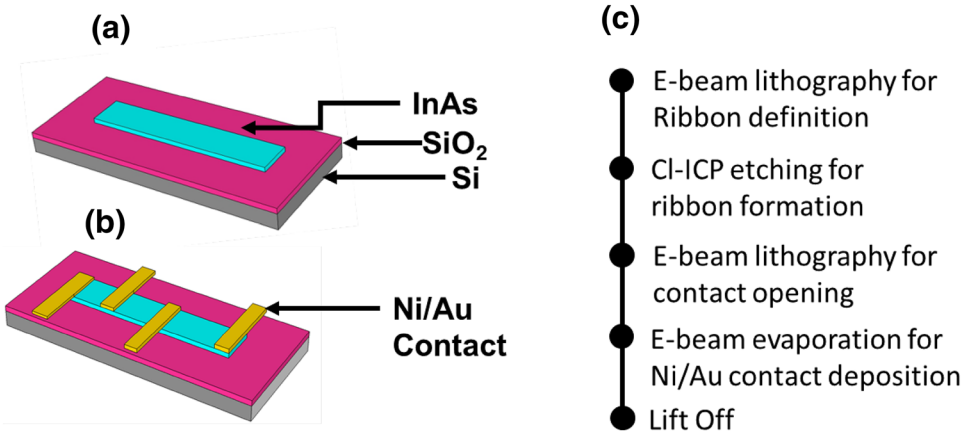

Fig. 1 **a** Schematic of InAs nano ribbons; **b** TLM structure on Si/SiO_2 substrate; **c** fabrication process flow of InAs TLM structures

transfer process. Through the standard photolithography method, patterns with 10 µm line width and 5 µm pitch were formed on InAs films on GaSb substrate using AZ MIR 701 photoresist. After that, the material was dipped into a mixed solution of citric acid, water and hydrogen peroxide ($C_6H_8O_7$: H_2O: H_2O_2 = 50 mg: 50 ml: 10 ml) to etch InAs film into ribbon arrays. Ammonium hydroxide solution (NH_4OH: H_2O = 10 ml: 90 ml) was then employed to selectively etch the underlying AlGaSb layer forming an undercut structure, which is beneficial to release the InAs ribbons from GaSb substrate during the following transfer step. Next, elastomeric PDMS slab was used to lift off the ribbons from the donor substrate and transfer the ribbons on Si/SiO_2 substrate. Detailed transfer procedure of InAs to Si/SiO_2 substrate has been described in [21]. The schematic diagram of a transferred InAs ribbon on Si/SiO_2 substrate is displayed in Fig. 1a.

Transmission line measurement structures were then fabricated on the transferred InAs ribbon on Si/SiO_2 substrate to investigate the effects of TFSI treatment on the electrical performances. Figure 1b and c exhibit the schematic diagram of the fabricated TLM structure on Si/SiO_2 substrate and the fabrication process flow, respectively. The transferred ribbons on Si/SiO_2 substrate were 20 nm thick and 60–100 µm long. The width of ribbons was first defined to be 4 µm by e-beam lithography and chlorine chemistry-based (Cl: Ar = 5: 15) inductively coupled plasma (ICP) dry etching. Hydrogen silsesquioxane (HSQ) was used as EBL resist and the dry etching mask. Next, the samples were dipped into diluted HF (HF: DI = 2: 98) for 120 s to remove HSQ. To put metal contacts, bi-layer EBL and lift-off techniques were used with MMA/PMMA bi-layer resist. Samples were treated with diluted HF (HF: DI = 1: 99) to remove the native oxide. Ultimately, Ni/Au (40 nm/15 nm) stack was used as contact metals. The contact area on the semiconductors is designed to be 4×4 µm^2. The distances between contacts were designed

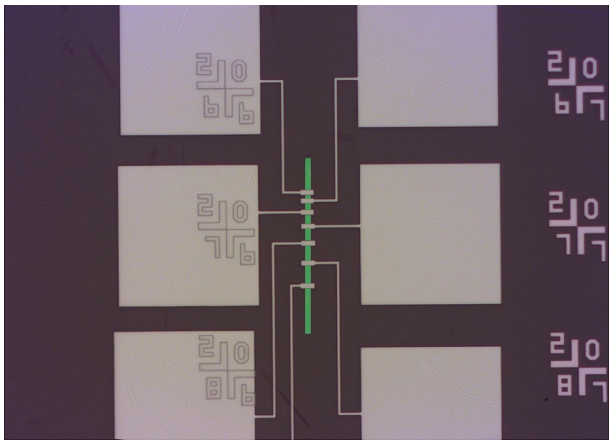

Fig. 2 Optical microscope image of fabricated TLM structure on InAs nanoribbon. The contacts are fabricated at 2-micron incremental step starting at 2 microns (InAs is in Green, and contacts are in white)

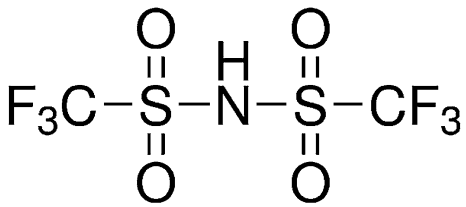

Fig. 3 Chemical structure of bis(trifluoromethane) sulfonamide

to be 2, 4, 6, 8 and 10 microns. Figure 2 shows the optical microscope image of the fabricated InAs TLM structure.

To do the surface treatment, we have used bis(trifluoromethane) sulfonamide (TFSI). TFSI is solid at room temperature and hence must be dissolved in a solvent before treatment. The chemical structure of TFSI is shown in Fig. 3. To prepare the TFSI solution, 1, 2-dichloroethene (DCE) and 1, 2-dichlorobenzene (DCB) were chosen as a solvent. The treatment procedure with TFSI is as follows:

24 mg TFSI powder was dissolved in 12 ml of 1, 2-dichloroethene (DCE) to make a 2 mg/ml solution. 0.5 ml of this solution was further diluted with 4.5 ml 1, 2-dichlorobenzene (DCB) to make a 0.2 mg/ml TFSI solution. The InAs ribbons are immersed in the 0.2 mg/ml solution for 20 s and then blew dry with N_2 for 30 s. Figure 4 depicts the schematic diagram of TFSI treatment.

3 Results and discussion

Transmission line measurement (TLM) was performed to analyze the effect of TFSI treatment on the sheet resistance and contact resistance between semiconductor and metal. HP 4156B Parameter analyzer equipped with Kelvin probes were used to measure the TLM structures. Kelvin set-up was used to eliminate any parasitic resistances. Figure 5a shows the current–voltage characteristics of the TLM structure with 6 μm distance before and after TFSI treatment. Initial measurement shows a perfect ohmic relationship between the InAs and metal contact (Red). After super acid treatment, the current–voltage characteristics of the InAs ribbon become nonlinear (blue).

Figure 5b shows the total resistance as a function of the distance between contacts of the InAs TLM structure before TFSI treatment. As the current–voltage characteristic becomes nonlinear after TFSI treatment, the transmission line data could not be extracted. From the transmission line data, the contact resistance and sheet resistance before TFSI treatment are 391.665 Ω and 465.72 Ω/□, respectively. To shed light on the mechanism of electronic characteristic changes on the InAs surface, we performed

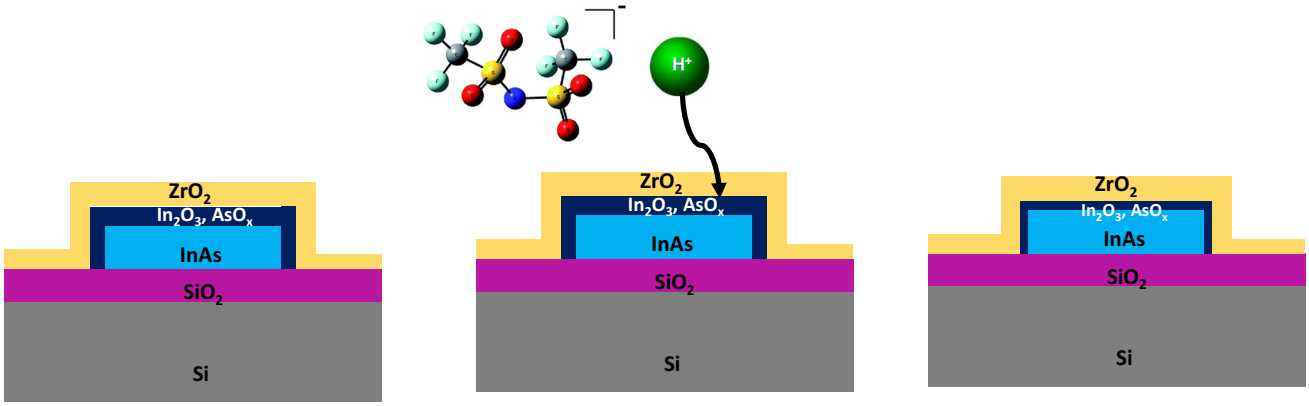

Fig. 4 Schematic diagram of TFSI treatment and In_2O_3 reduction process

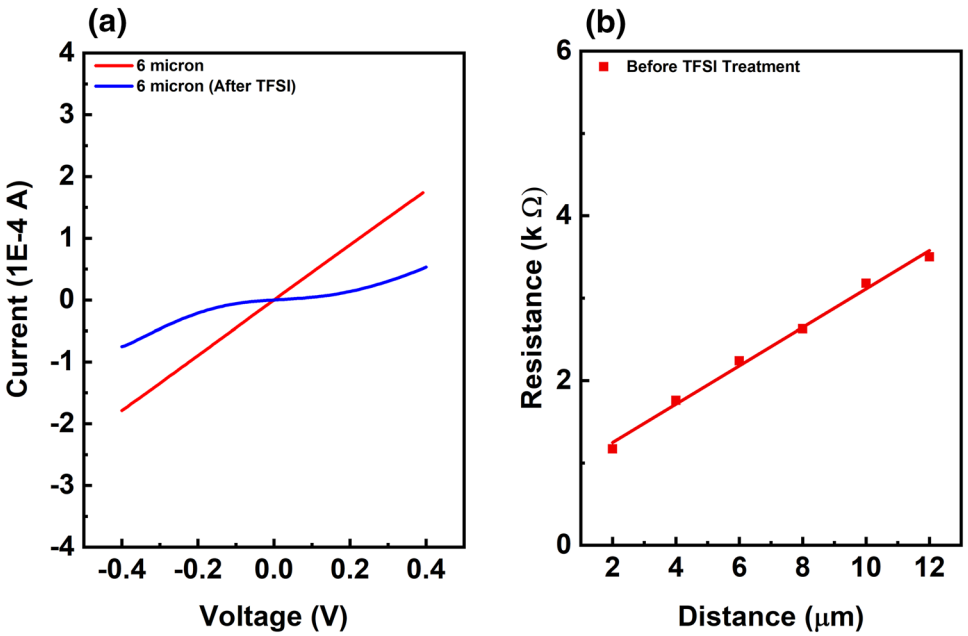

Fig. 5 **a** Current–voltage characteristics of InAs TLM structure after different conditions. Before any treatment (red), the graph is perfectly linear and shows ohmic characteristics; After TFSI treatment (blue), the InAs exhibits Schottky characteristics; **b** transmission measurement data before any treatment (red); After TFSI treatment, the current–voltage characteristic become nonlinear, so the resistance value could not be extracted

X-ray photoelectron spectroscopy (XPS) measurements. TFSI in DCE solution contains a large number of hydrogen ions and negative molecular chains. The molecular chains would remain on the surface of InAs after TFSI treatment [22]. Figure 6 shows the XPS survey scan spectra before (red) and after (black) TFSI treatment. From Fig. 6, it can be seen that elements such as fluorine and sulfur appear in the XPS spectra after TFSI treatment. These elements are also present in the chemical structure of the TFSI in Fig. 3 manifesting that the molecular chains remain on the surface of InAs after TFSI treatment.

Ohmic contacts between metal and semiconductor have been studied extensively [23, 24]. Whether a given metal–semiconductor junction is an ohmic contact or a Schottky barrier depends on the Schottky barrier height, Φ_B, of the junction. The Schottky barrier is calculated from the vacuum work function of the metal relative to the vacuum electron affinity of the semiconductor and follows the following equation:

$$q\varphi_B = q(\varphi_m - \chi),$$

where $q\varphi_m$ is the work function of metal and $q\chi$ is the electron affinity of the semiconductor material. For a sufficiently large Schottky barrier height, the semiconductor and the metal behave as a Schottky barrier. For a lower barrier height (such as the case of InAs, $q\chi = 4.9$ eV and nickel, $q\varphi_m = 5.01$ eV), the semiconductor and the metal form ohmic contact instead of Schottky barrier. This is due to a phenomenon called Fermi-level pinning. Fermi-level pinning occurs due to the surface states which are distributed in energy within the bandgap of the semiconductor. These surface states have a high density at a certain energy level known as neutral level. This neutral level tends to pin the Fermi level in the semiconductor leading to weak dependence of the barrier height on the metal work function [25, 26].

When the TLM structures were passivated with TFSI, the surface of the InAs and Ni–InAs contact got affected in several ways. The Hammett number of TFSI in DCE solvent is known to be extremely high (~ 10^{10} times higher than nitric and sulfuric acid [7]), meaning the TFSI molecule acts as an excellent proton [H+] source. The H+ adsorption on nickel surfaces causes an immediate decrease in conductivity and an increase in work function [27]. The large negative molecular chains of TFSI accumulated on the surface of the InAs semiconductor surface also affects the surface states of the semiconductor manifesting a Schottky-like non-linearity in InAs TLM result.

Figure 7a and b shows the measured and calibrated XPS spectra of the element oxygen 1 s peak before and after the TFSI treatment, respectively. The obvious asymmetry of the measured oxygen peak in both spectra implies the existence of different oxides. The peak at 529.7 eV corresponds to In_2O_3 while the peak at 531.5 eV corresponds to AsO_x (mix of As_2O_3 and AS_2O_5) [28–30]. After TFSI treatment, the intensity of AsO_x remains almost constant, while the intensity of In_2O_3 reduces greatly. The integral intensity ratio between AsO_x and In_2O_3 has increased from 1.34 to 3.13 with TFSI treatment. The result manifests that the native oxide of InAs, especially In_2O_3, can be effectively reduced after TFSI treatment.

Although TFSI treatment can reduce the native oxide, namely In_2O_3, from the surface of InAs, the adverse Schottky behavior (due to the presence of larger TFSI molecule on the InAs surface and degradation of Ni contact) restricts the TFSI to be applied as a direct surface treatment method. To solve this problem, we introduced a thin layer of amorphous metal oxide on top of the TLM structure. The H+ could easily diffuse through the amorphous oxide layer

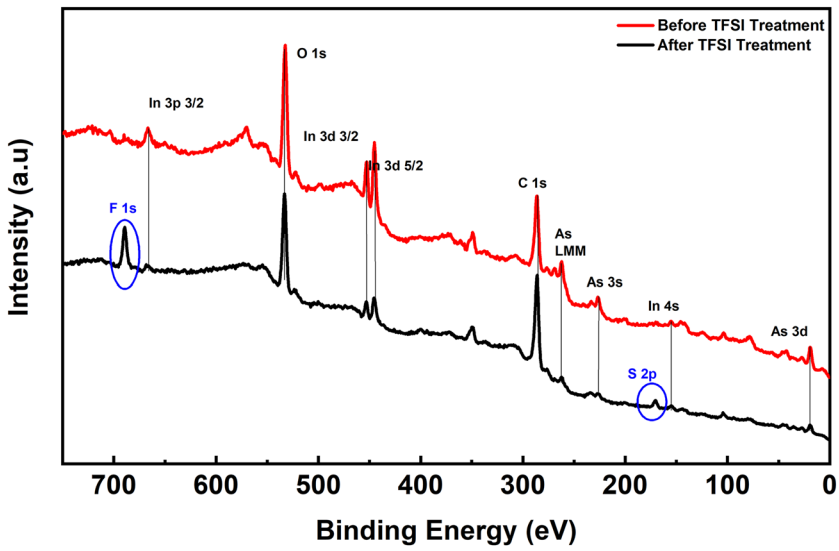

Fig. 6 XPS line scan survey spectra before (red) TFSI treatment after (black) TFSI treatment

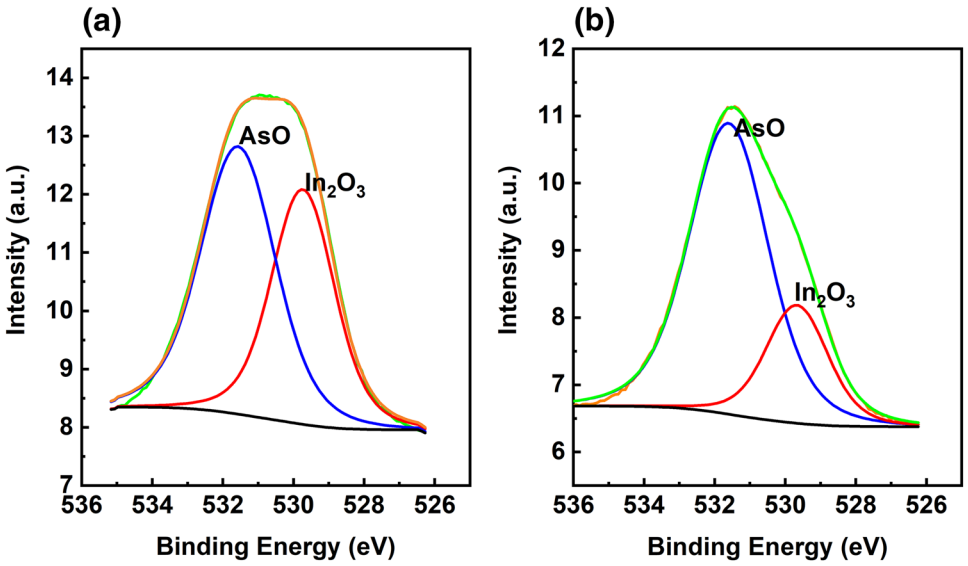

Fig. 7 Oxygen 1 s XPS spectrum of **a** InAs before super acid treatment showing relative intensity of AsO and In_2O_3; **b** After super acid treatment, the spectra shows the relative intensity of AsO to In_2O_3

while the larger TFSI molecule cannot. This will protect the InAs surface from becoming contaminated with larger TFSI molecule. The amorphous oxide layer will also lessen the degradation of the Ni contact significantly. To investigate the effect of TFSI on amorphous oxide-protected InAs surface and Ni–InAs contact, we fabricated another batch of TLM devices following the procedure mentioned above. After fabricating the TLM device, we deposited 8-nm ZrO_2 by atomic layer deposition (ALD) at 130 °C. Figure 8 shows the current–voltage characteristics of the ZrO_2-protected TLM device before and after TFSI treatment. From the figure, we can see that, after TFSI treatment the sheet resistance decreases from 682 Ω/□ to 478 Ω/□. The contact resistance after TFSI treatment is only 13.45 Ω. From the sheet resistance and contact resistance calculation before and after TFSI treatment, it is clear that ZrO_2 protected the surface from the larger TFSI molecule while the H + penetrates through. The reduction in sheet resistance is, therefore, due to the reduction in In_2O_3 at the InAs/oxide interface.

One of the most challenging aspects of the integration of III–V materials with silicon process is the surface quality of the III–V semiconductors. The surface quality has a far-reaching influence on the performance of III–V MOSFETs. TFSI treatment is a novel surface treatment process which can effectively reduce the native In_2O_3 and improve the surface quality. Hence, this method is expected to be

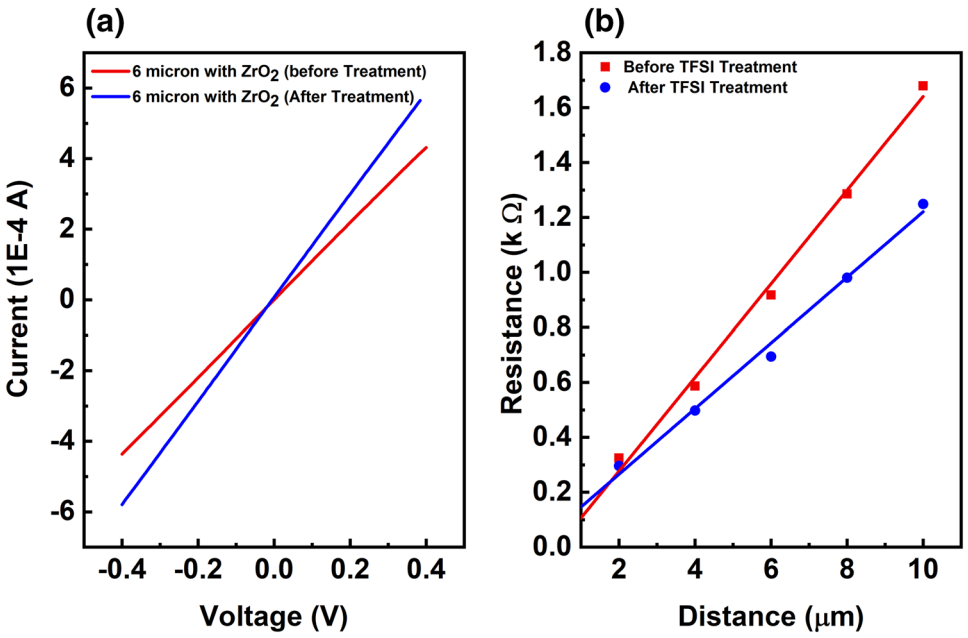

Fig. 8 Current–voltage characteristics of InAs TLM structure encapsulated by ZrO_2. **a** Red line shows the characteristics before TFSI treatment and the blue line shows the characteristics after TFSI treatment. Both curves exhibit linear relationship; **b** Transmission measurement data before (red) and after (blue) the TFSI treatment

able to improve other III–V material-based MOSFETs which contain indium such as InP, InSb, InAs, InGaAs, InGaP, InGaSb, and InAsSb. Another unique attribute of this surface treatment process is that, it can be applied to the devices without significantly changing any established fabrication process. As the TFSI treatment works at the presence of the amorphous oxides such as ZrO_2 and penetrates through the amorphous oxide, it can be used as a post-fabrication surface treatment process to improve the surface quality of the III–V materials.

4 Conclusions

In summary, we have investigated the effect of TFSI treatment on InAs material and Ni–InAs contacts. TFSI treatment can effectively reduce the native oxide, especially In_2O_3 from the surface of InAs. But the nonlinear current–voltage characteristics suggest that the TFSI cannot be used as a direct surface treatment method. Hence, we established a process to eliminate the nonlinear current–voltage characteristics by employing amorphous oxide such as ZrO_2. We have demonstrated that TFSI can reduce the native oxide such as In_2O_3 from ZrO_2 passivated InAs surface. Therefore, this novel passivation method could be used in III–V MOSFET fabrication process flow as the final step and enhance device performances.

References

1. D.H. Kim, J.A. del Alamo, I.E.E.E. Trans, Electron Devices **57**, 1504 (2010)
2. J.A. del Alamo, Nature **479**, 317 (2011)
3. M. Heyns, W. Tsai, MRS Bull. **34**, 485 (2009)
4. M. Cooke, Semicond. TODAY Compd. Adv. Silicon **11**, 4 (2016)
5. H. Riel, L. Wernersson, M. Hong, J.A. del Alamo, MRS Bull. **39**, 668–677 (2014)
6. K. Takei, R. Kapadia, H. Fang, E. Plis, S. Krishna, J. Ali, Appl. Phys. Lett. **102**, 153513 (2013)
7. Y.-C. Fu, U. Peralagu, D.A.J. Millar, J. Lin, I. Povey, X. Li, S. Monaghan, R. Droopad, P.K. Hurley, I.G. Thayne, Appl. Phys. Lett. **110**, 142905 (2017)
8. D.M. Zhernokletov, H. Dong, B. Brennan, J. Kim, R.M.A. Wallace, J. Vac. Sci. Technol. B Nanotechnol. Microelectron. Mater. Process. Meas. Phenom. **30**, 04E103 (2012)
9. M.V. Lebedev, E.V. Kunitsyna, W. Calvet, T. Mayer, W. Jaegermann, J. Phys. Chem. C **117**, 15996–16004 (2013)
10. H. Lim, C. Carraro, R. Maboudian, M.W. Pruessner, R. Ghodssi, Langmuir **20**, 743–747 (2004)
11. C.L. McGuiness, A. Shaporenko, C.K. Mars, S. Uppili, M. Zharnikov, D.L. Allara, J. Am. Chem. Soc. **128**, 5231–5243 (2006)
12. H.A. Budz, M.C. Biesinger, R.R.J. LaPierre, Vac. Sci. Technol. B Microelectron. Nanometer Struct. Process. Meas. Phenom. **27**, 637 (2009)
13. X. Ding, K. Moumanis, J.J. Dubowski, L. Tay, N.L. Rowell, J. Appl. Phys. **99**, 054701 (2006)
14. S. Ye, G. Li, H. Noda, K. Uosaki, M. Osawa, Surf. Sci. **529**, 163–170 (2003)
15. D. Cuypers, C. Fleischmann, D.H. van Dorp, S. Brizzi, M. Tallarida, M. Müller, P. Hönicke, A. Billen, R. Chintala, T. Conard, Chem. Mater. **28**, 5689–5701 (2016)
16. A. Kütt, T. Rodima, J. Saame, E. Raamat, V. Maemets, I. Kaljurand, I.A. Koppel, R.Y. Garlyauskayte, Y.L. Yagupolskii, L.M. Yagupolskii, E. Bernhardt, H. Willner, I. Leito, J. Org. Chem. **76**(2), 391–395 (2011)
17. Z. Liu, Y. Sun, F. Machuca, P. Pianetta, W.E. Spicer, R.F.W. Pease, J. Vac. Sci. Technol. B **2003**, 21 (1953)
18. N.J. Kadhim, S.H. Laurie, D. Mukherjee, J. Chem. Educ. **75**(7), 840 (1998)
19. R. Vos, S. Arnauts, T. Conard, A. Moussa, H. Struyf, P.W. Mertens, Solid State Phenom. **187**, 27–31 (2012)
20. M. Aman, D.H. Lien, D. Kiriya, J. Xiao, A. Azcatl, J. Noh, S.R. Madhvapathy, R. Addou, K.C. Santosh, M. Dubey, K. Cho, R.M. Wallace, S.C. Lee, Jr-HW Ager III, X. Zhang, E. Yablonovitch, A. Javey, Science **350**(6264), 1065–1068 (2015)
21. H. Ko, K. Takei, R. Kapadia, S. Chuang, H. Fang, P.W. Leu, K. Ganapathi, E. Plis, H.S. Kim, S.Y. Chen, M. Madsen, A.C. Ford, Y.-L. Chueh, S. Krishna, S. Salahuddin, A. Javey, Nature **468**, 286–289 (2010)
22. J. Bullock, D. Kiriya, N. Grant, A. Azcatl, M. Hettick, T. Kho, P. Phang, H.C. Sio, D. Yan, D. Macdonald, M.A. Quevedo-Lopez, R.M. Wallace, A. Cuevas, A. Javey, ACS Appl. Mater. Interfaces. **8**(36), 24205–24211 (2016)
23. H.K. Henisch, *Rectifying Semiconductor Contacts* (Clarendon Press, Oxford, 1957)
24. E.H. Rhoderick, *Metal-Semiconductor Contacts* (Clarendon Press, Oxford, 1977)
25. S.M. Sze, K.K. Ng, *Phyics of Semiconductor Devices* (Wiley, Hoboken, 2007)
26. E.H. Rhoderick, Metal-semiconductor contacts, in IEE Proceedings, vol. 129 (**1982**)
27. W.M.H. Sachtler, J. Chem. Phys. **25**(4), 751–752 (1956)
28. M. Procop, J. Electron Spectros. Relat. Phenom. **59**, R1 (1992)
29. M. Losurdo, M.M. Giangregorio, F. Lisco, P. Capezzuto, G. Bruno, S.D. Wolter, M. Angelo, A. Brown, J. Electrochem. Soc. **156**, H263 (2009)
30. G. Hollinger, R. Skheyta-Kabbani, M. Gendry, Phys. Rev. B **49**, 11159 (1994)